Catalysis Today 164 (2011) 364–369

Contents lists available at ScienceDirect

Catalysis Today

journal homepage: www.elsevier.com/locate/cattod

Synthesis and characterization of novel SiO_2 and TiO_2 co-pillared montmorillonite composite for adsorption and photocatalytic degradation of hydrophobic organic pollutants in water

Jiangyao Chen[a,c], Xiaolu Liu[a,c], Guiying Li[a], Xin Nie[a,c], Taicheng An[a,*], Shanqing Zhang[b], Huijun Zhao[b]

[a] State Key Laboratory of Organic Geochemistry, Guangdong Key Laboratory of Environmental Resources Utilization and Protection, Guangzhou Institute of Geochemistry, Chinese Academy of Sciences, Guangzhou 510640, China
[b] Environmental Futures Centre and Griffith School of Environment, Gold Coast Campus, Griffith University, QLD 4222, Australia
[c] Graduate School of Chinese Academy of Sciences, Beijing 100049, China

ARTICLE INFO

Article history:
Received 2 July 2010
Received in revised form 29 October 2010
Accepted 2 November 2010
Available online 3 December 2010

Keywords:
Pillared montmorillonite
Adsorption
Photocatalysis
2,4,6-Trichlorophenol
Degradation mechanism

ABSTRACT

A series of SiO_2 and TiO_2 co-pillared montmorillonite photocatalysts with excellent adsorption capacity and high photocatalytic activity were synthesized via a sol–gel method by pillaring both SiO_2 and TiO_2 mixed sol into sodium montmorillonite. Various material characterization techniques such as powder X-ray diffraction (XRD), nitrogen adsorption/desorption isotherms and scanning electron microscopy (SEM) were used to examine the pillared montmorillonites. 2,4,6-trichlorophenol, a typical hydrophobic organic pollutant, was used as a model pollutant to evaluate the adsorption capacity and photocatalytic activity of the prepared co-pillared montmorillonites. The experimental results showed that large SiO_2 content in the pillared montmorillonite was in favor of large adsorption capacity, while large TiO_2 content in the co-pillared montmorillonite was beneficial for the high photocatalytic activity, and the highest photocatalytic activity was obtained for the prepared co-pillared montmorillonite with a SiO_2/TiO_2 molar ratio of 1:2. Additionally, nine intermediates including 2,4-dichlorophenol, 2-chloro-1,5-diphenol, 1,3,7-trichlorodibenzo-p-dioxin, 2,6-dichlorodibenzo-p-dioxin, hexadiene diacid, butyl alkyd, oxalic acid, phloroglucinol and diphenol were detected, and a photocatalytic degradation mechanism of TCP was tentatively proposed.

1. Introduction

Up till now, titanium dioxide (TiO_2) has been the dominant photocatalyst for environmental application due to its superior photocatalytic oxidation ability, nonphotocorrosive, nontoxic, and inexpensive characteristics [1–3]. Nevertheless, there are still some inherent drawbacks, such as small specific surface area and low adsorption ability inhabiting its practical application [4]. The intercalation of TiO_2 and other inorganic cations into the interlayer of montmorillonite is one of the most promising methods to improve the adsorption performance and the photocatalytic activity of organic pollutants. As reported, TiO_2 pillared montmorillonite displayed larger specific surface area [5], higher selectivity [6] and better adsorption ability [7] to hydrophobic organic pollutants than that of pure TiO_2. However, TiO_2 particles pillared in montmorillonite are often in amorphous phases, resulting in low photocatalytic activity. Furthermore, most of the prepared TiO_2 pillared montmorillonites (TiPM) have poor adsorption capability due to their small basal spacing. The synthesis of the TiPM with large adsorption capacity and high photocatalytic activity is still a challenging topic in this field.

Recently, the preparation of SiO_2 and TiO_2 co-pillared montmorillonite (SiTiPM) has been attracting extensive interests because it is possible to obtain the pillared montmorillonite with both large adsorption capacity and high photocatalytic activity. Choy et al. [8] first intermixed SiO_2 and TiO_2 nanoparticles into the interlayer space of montmorillonite, and found from the N_2 adsorption–desorption data that these pillared montmorillonite could be used as good adsorptive support for catalyst without considering activity. Ding et al. [9] also prepared TiPM and SiTiPM to compare their activities in the photocatalytic degradation of phenol, and the results showed that the photocatalytic activity of SiTiPM was much lower than that of TiPM when the contribution of the adsorption was not considered. Although some SiTiPM composite materials were synthesized previously by other researchers [8,9], the dependence of photocatalytic activity on the adsorption performance of SiTiPM has not been investigated. More recently, we [10] prepared a novel TiO_2 immobilized hydrophobic montmorillonite photocatalyst which could effectively enhance the adsorption and degradation efficiencies of decabromodiphenyl

* Corresponding author. Tel.: +86 20 85291501; fax: +86 20 85290706.
E-mail address: antc99@gig.ac.cn (T. An).

0920-5861/$ – see front matter © 2010 Elsevier B.V. All rights reserved.
doi:10.1016/j.cattod.2010.11.014

ether, a typical hydrophobic organic pollutant, in water. Meng et al. [11] also immobilized mixed SiO_2 and TiO_2 nanoparticle onto hydrophobic montmorillonite to synthesize SiO_2/TiO_2-organoclay hybrids, which possessed both large adsorption capability and high photocatalytic activity to hydrophilic organic pollutant, methyl orange, in water. Therefore, it can be concluded that regardless of hydrophobic or hydrophilic property of the organic pollutants, the adsorption capacity of the catalysts play a very important role in their photocatalytic activity of these pillared or immobilized montmorillonite composites. Thus, the relationship between the adsorption performance and the photocatalytic activity of the SiTiPM catalyst for hydrophobic or hydrophilic organic pollutants should be investigated.

In this work, we synthesize a series of novel SiTiPM photocatalysts with different ratios of SiO_2 to TiO_2 to degrade hydrophobic organic pollutants. The main objective is to investigate the influence of the adsorption performance on the photocatalytic activity of prepared SiTiPMs. To achieve this, the adsorption and photocatalytic behaviors of organic pollutants at the SiTiPM were systematically evaluated by using the newly prepared SiTiPM as the photocatalyst. 2,4,6-trichlorophenol (TCP) was selected as a model of hydrophobic organic pollutants, because of its toxic properties, long half life, lipophilicity, bioaccumulation, and widespread distribution. To better understand its environmental fate and the transformation of TCP onto these prepared SiTiPMs, a photocatalytic degradation mechanism of TCP was also tentatively proposed based on the identified intermediates.

2. Materials and methods

2.1. Reagents and apparatus

Raw montmorillonite (RM) was obtained from Lin'an (LA), Zhejiang, China, while Tetra-n-butyl titanium (98%, $Ti(OC_4H_9)_4$) and tetraethylorthosilicate (98%) were all purchased from Tianjing Damao Chemical Reagent Factory, China. 2,4,6-trichlorophenol (TCP, 99%), was obtained from Fluka (Taufkirchen, Germany). All other reagents were analytic grade, and all aqueous solutions were prepared with deionized water.

X-ray diffraction (XRD) patterns were recorded on a Rigaku Dmax X-ray diffractometer with Cu Kα radiation. Nitrogen adsorption/desorption isotherms were obtained at 77 K with a Micromeritics ASAP 2020 system. Scanning electron microscope (SEM, SU-1500) was used to obtain the crystal microstructure and size of the prepared pillared montmorillonites.

2.2. Preparation of pillared montmorillonites

A 50 g RM was dispersed into 1 L of deionized water under vigorous stirring, and then 0.4 L of 0.43 mol/L NaCl solution was slowly added into the suspension. After being stirred at 80 °C for 3 h, the resultant mixture was stirred for another 12 h at room temperature. Then the suspension was isolated by a centrifuge, and washed with deionized water to remove the excess chloride ions. Sodium montmorillonite (NaPM) was obtained after the sample was dried at 100 °C for 24 h.

In a typical synthesis procedure of TiPM, a mixture containing 10 g of $Ti(OC_4H_9)_4$ and 15 mL of ethanol was added dropwise to 60 mL acetic acid solution (20%, v/v) under vigorous stirring. The mixture was sealed and stirred for 2 h and then was slowly added into 1 wt% of NaPM suspension and stirred for another 24 h. The molar ratio of TiO_2 to cation-exchange capacity (CEC) was 40:1. For SiPM, SiO_2 sol was also prepared by hydrolysis of 10.9 g $Si(OC_2H_5)_4$) with 3 mL acetic acid solution and 5 mL ethanol. After stirring for 2 h, the pure SiO_2 sol was added to 1 wt% of NaPM suspension and stirred for another 24 h. The molar ratio of SiO_2 to CEC was also 40:1. As for SiTiPM, it was prepared by mixing 1 wt% NaPM suspension with TiO_2 sol and SiO_2 sol with the molar ratios of 2:1, 1:1 and 1:2. The wet solid was obtained after centrifugation and triplet washing with deionized water, and then was dried at 100 °C and finally calcinated at 450 °C for 4 h. These three prepared SiTiPM were labeled as $SiTiPM_{21}$, $SiTiPM_{11}$ and $SiTiPM_{12}$, respectively.

2.3. Isothermal adsorption test

Isothermal adsorption experiments were performed by allowing 0.1 g of various pillared montmorillonites and 50 mL TCP solution to reach the adsorption equilibrium. The initial concentrations of TCP ranged from 5 to 150 mg/L. After reaching adsorption equilibrium, the resulting suspension was separated by centrifuge and the supernatant was collected for subsequent analysis.

2.4. Photocatalytic activity and analytical methods

The photocatalytic activities of the prepared TiO_2 or pillared montmorillonites were tested by the degradation of TCP with the initial concentration of 20 mg/L. The detail photocatalytic experiments were described in our previous publication [12]. The concentrations of TCP were measured by an UV–Vis spectrophotometer (HEλIOS α) at a wavelength of 293 nm. For the intermediates analysis, filtered solutions were extracted by redistilled CH_2Cl_2 three times and the extracted liquid was dried under N_2 blowing. Before analysis, some dry samples were rediluted into 200 μL hexane and the rest was silylated in 50 μL of bis(trimethylsilyl)trifluoroacetamide (BSTFA) in a sealed vial overnight with 50 μL pyridine as catalyst. The intermediates were identified by gas chromatography/mass spectrometry (GC/MS, HP 6890, Micromass Platform II) equipped with a HP-5 capillary column (30 m × 0.32 mm × 0.25 μm, Agilent Technology). The injector and the ion source temperature were 230 °C and 270 °C, respectively. The temperature program: 80 °C (8 min), 80–295 °C at 10 °C/min. The MS was operated in full scan mode with m/z 40–300 amu. Data acquisition and processing were controlled by a HP Chemstation data system.

3. Results and discussion

3.1. Characterization

The small angle XRD patterns of RM and NaPM are shown in Fig. S1. The RM and NaPM display the (0 0 1) diffraction peak at 6.82° and 7.12°, respectively, indicating that the basal spacing of the montmorillonite shrinks from 1.296 to 1.242 nm after being exchanged with Na^+ which can be estimated by the Bragg formula. It is also found that the diffraction peak of montmorillonite becomes sharper reflecting the uniform pore structure forms [13].

The wide angle XRD patterns of the prepared TiO_2 and various pillared montmorillonite are also shown in Fig. 1. It can be found that the XRD pattern of SiPM exhibits very similar characteristic peaks as that of NaPM, indicating that the SiPM has a similar structure as NaPM. This is because that Na^+ was exchanged by Si^{4+} with the similar element radius. Nevertheless, the characteristic peaks of NaPM at $2\theta = 20.9°$ and 26.7°, which are consistent with those of SiO_2 (JCPDS No. 46-1045), are weakened remarkably for the pillared montmorillonites, implying that the layer structures of these pillared montmorillonites are almost destroyed and SiO_2 pillars existed in amorphous phase. No obvious diffraction peaks of TiO_2 anatase ($2\theta = 25.3°$) can be found in XRD patterns of both $SiTiPM_{21}$ and $SiTiPM_{11}$ samples possibly because the contents of TiO_2 in these two pillared montmorillonites are too low to be detected by the XRD [9]. With the increase of the TiO_2 content, an obvious anatase

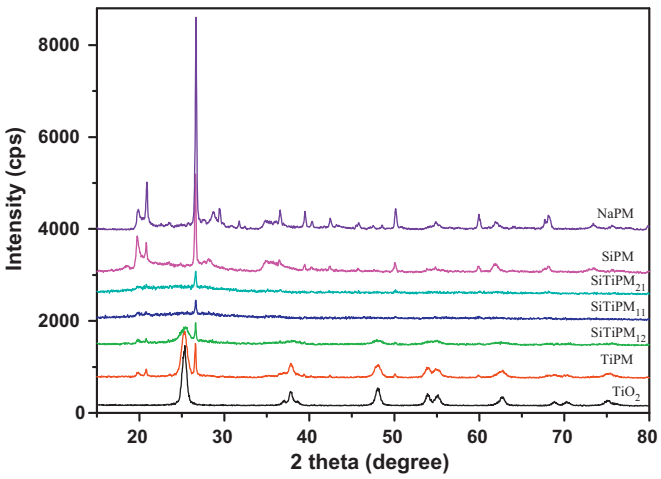

Fig. 1. Wide angle XRD patterns of the prepared samples.

characteristic peak at $2\theta = 25.3^\circ$ can be observed for $SiTiPM_{12}$. From TiO_2, TiPM to $SiTiPM_{12}$, the characteristic peak at $2\theta = 25.3^\circ$ broadens gradually. According to the calculation, the average crystal sizes of anatase TiO_2 were 15.3, 12.1 and 10.9 nm, respectively. This is due to the fact that the insertion of certain SiO_2 into TiO_2 particles can reduce the size of TiO_2 particles in the pillar, which makes it possible to prepare better catalyst with high photocatalytic activity [14].

Nitrogen adsorption/desorption isotherms and Barrett–Joyner–Halenda (BJH) pore size distribution of the RM and NaPM are illustrated in Fig. S2. It is apparent to find that the shapes of the isotherms are similar (not a distinctive type IV) with H3 hysteresis loops [15] and the pore sizes are 3.69 and 3.56 nm for RM and NaPM, respectively (inset in Fig. S2). The results reveal that although the pores are almost the same, the pore size of the montmorillonite reduces gradually after the Na^+ pillared resulted in the shrinkage of the basal spacing.

As shown in Fig. 2, nitrogen adsorption/desorption isotherms and Barrett–Joyner–Halenda (BJH) pore size distribution of various TiPM, SiPM and SiTiPMs exhibit a type IV isotherm with different desorption hysteresises (IUPAC classification), indicating the existence of mesoporous structure [15]. TiPM exhibits a H1 hysteresis loop, implying that the pillared montmorillonite has relatively uniform pore size distribution [15]. Similar to NaPM, SiPM also shows a similar type IV isotherm with a typical H3 hysteresis loop providing evidence of similar structure with NaPM. All SiTiPMs exhibit wide, triangular and high-pressure hysteresis loops, which indicates the collapse of lamellar structures of montmorillonites and may give rise to highly similar adsorption capabilities [16].

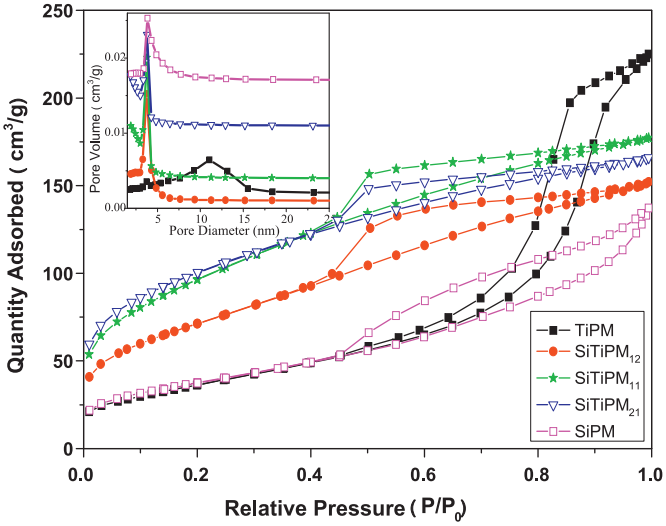

Fig. 2. The N_2 adsorption/desorption isotherms and BJH desorption pore size distributions of the pillared montmorillonites.

Table 1
The adsorption characteristics of the pillared montmorillonites.

Pillared montmorillonites	NaPM	TiPM	$SiTiPM_{12}$	$SiTiPM_{11}$	$SiTiPM_{21}$	SiPM
BJH total volume (cm^3/g)	0.0425	0.3351	0.2307	0.2711	0.2536	0.1901
BET surface area (m^2/g)	22.7	133.0	258.9	352.0	360.1	137.0

The average pore sizes of $SiTiPM_{21}$, $SiTiPM_{11}$, $SiTiPM_{12}$ and SiPM are calculated almost the same as 3.78, 3.78, 3.74 and 3.85 nm, respectively. Obviously, these pillared montmorillonites are mesoporous materials. In addition, the inset in Fig. 2 showed that the dominant pore sizes of SiTiPMs are much smaller than that of TiPM (11.06 nm), indicating that smaller sized TiO_2 particles may be formed in the smaller pores, resulting in better photocatalytic activity for SiTiPM.

The other adsorption parameters of prepared pillared montmorillonites are also listed in Table 1. It can be seen that with the increase of the molar ratio of SiO_2 to TiO_2 from 1:2, 1:1 to 2:1, the specific surface area of pillared montmorillonite increases from 258.9, 352.0 to 360.1 m^2/g, by companying with the pore volume changes from 0.2307, 0.2711 to 0.2536 cm^3/g, respectively. In contrast, the specific surface area of TiPM prepared by the similar procedure is only 133.0 m^2/g although its pore volume is 0.3351 cm^3/g which is much bigger than other pillared montmorillonites. Comparatively, the SiPM has the smallest pore volume (0.1901 cm^3/g) though the specific surface area (137.0 m^2/g) is just slightly larger than that of TiPM. This result is similar with the data reported by Endo et al., where the specific surface areas were found to be 40–190 m^2/g [17]. In this work, the SiPM still has a structure as the NaPM with the same order of the specific surface area (22.7 m^2/g) and pore volume (0.0425 cm^3/g). In addition, very similar XRD patterns and N_2 adsorption/desorption isotherms also clearly demonstrate similar results with SiPM. The possible reason is due to only partial SiO_2 successfully pillared into the montmorillonite. This is in line with previous observations that the silica sol was hardly pillared into the montmorillonite [18] and only a few amount of SiO_2 is responsible for the pillars [9].

The SEM images of the NaPM and pillared montmorillonites are shown in Fig. 3. The NaPM sample (see Fig. 3a) has compact and integrated lamellar structures, which may be suitable for preparation of regular pillared materials. The similar lamellar structures can also be easily found in the SiPM (see Fig. 3b) and TiPM samples (see Fig. 3f) although the structure of SiPM is more uniform. Moreover, the uniform size and distribution of the pores in the TiPM image verified well the N_2 adsorption/desorption results of the TiPM. For the SiTiPM, the lamellar structures of montmorillonite can hardly be found (Fig. 3c–e). However, more and more connective pores and integrated surface are formed with the increase of the content of SiO_2 in pillared montmorillonites from the $SiTiPM_{12}$ to $SiTiPM_{21}$, suggesting that higher specific surface area and better adsorption capacity can be obtained, which can be well supported by the results of nitrogen adsorption/desorption and isotherm adsorption experiments.

3.2. Isothermal adsorption and photocatalytic degradation of TCP

Dark adsorption for 12 h is conducted after adding the prepared pillared montmorillonites into the TCP solution to ensure that the

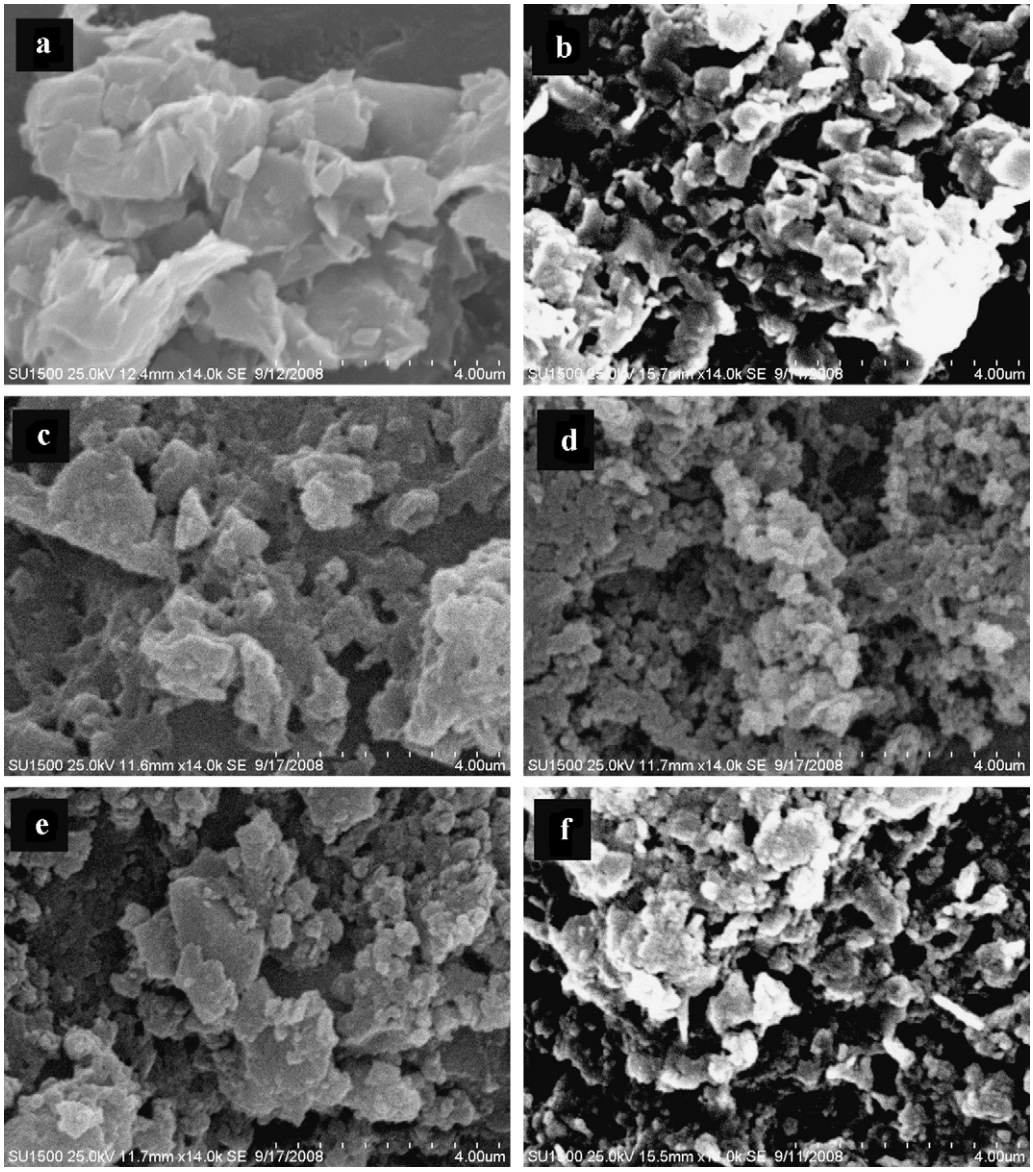

Fig. 3. SEM images of the montmorillonite samples ((a) NaPM; (b) SiPM; (c) $SiTiPM_{21}$; (d) $SiTiPM_{11}$; (e) $SiTiPM_{12}$; (f) TiPM).

adsorption equilibrium is achieved. The adsorption isotherms of TCP on different pillared montmorillonites are displayed in Fig. 4. It is obviously found that with increasing the molar ratio of SiO_2 to TiO_2 from 0 to 2.0, the adsorption capacity of TCP on pillared montmorillonites increases from 2.55 to 3.01 mg/g which is consistent with the increasing trend of specific surface area of pillared montmorillonites. Notably, the SiPM shows the best adsorption capacity of 6.48 mg/g although its specific surface area is not the largest among all pillared montmorillonites. It is because that the adsorption of organic pollutants onto montmorillonites is affected not only by the hydrophobicity but also the polarity of the adsorbents, i.e., TCP. Interlayer surface of the pillared montmorillonites is well known as hydrophobic after pillared [19,20]. It is also reported that the hydrophilicity of zeolites decreased significantly after Si^{4+} treatment [21] and the zeolites with a high Si/Al ratio became more hydrophobic [22]. Thus, with the increase of the SiO_2 content in the pillared montmorillonites, the hydrophobicity of the pillared montmorillonites will be enhanced, which results in the increase of adsorption capacity for hydrophobic TCP with the order of TiPM < $SiTiPM_{12}$ < $SiTiPM_{11}$ < $SiTiPM_{21}$ < SiPM. On the other hand, the SiO_2 pillared montmorillonite may possess additional polar-

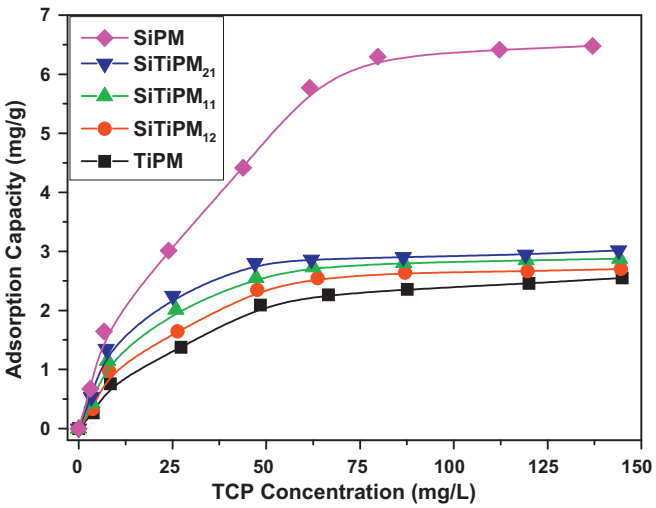

Fig. 4. The TCP adsorption isotherms at the pillared montmorillonite samples.

ity because SiO_2 is a dominant chemical composite [9] and polar structure [23]. In other words, the higher content of SiO_2 can lead to the stronger polarity of pillared montmorillonite. Thus, polar TCP can be therefore easier adsorbed and accumulated on SiPM than other pillared montmorillonites. The adsorption results indicate that the SiO_2 pillared montmorillonites display higher affinity toward the hydrophobic and polar organic pollutants, such as TCP.

Photocatalytic degradation kinetics of TCP at pure TiO_2 and pillared montmorillonites are shown in Fig. 5. The pure TiO_2 and TiPM show an excellent photocatalytic activity, and the removal efficiencies are both beyond 98% within 120 min. In contrast, the photocatalytic activities of SiTiPM are relatively weaker, but the adsorption capabilities of the SiTiPM are actually enhanced by the addition of SiO_2. According to the XRD analysis and photocatalytic results, it is found that an optimum molar ratio of SiO_2 to TiO_2 for SiTiPM with both high adsorption ability and photocatalytic activity was 1:2. If the ratio is out of this optimum range, for instance, it equals to 1:1 or 2:1, the removal efficiencies of TCP are only 14.4% ($SiTiPM_{11}$) and 7.8% ($SiTiPM_{21}$) within 120 min, respectively. The possible reason for this is that some of TiO_2 nanoparticles were surrounded by extra SiO_2 and the prepared pillared montmorillonite, leading to lower photocatalytic activity. When the molar ratio of SiO_2 to TiO_2 is within this optimum range such as 1:2, $SiTiPM_{12}$ exhibits relatively higher photocatalytic activity and the degradation efficiency of TCP can reach 40% within 120 min. From this experiment we can find that although the prepared SiTiPMs have much lower photocatalytic activity than the TiO_2 pillared montmorillonite, the high adsorption performance of these prepared composites still plays a very important role in the degradation of low level hydrophobic organic pollutants in water environment.

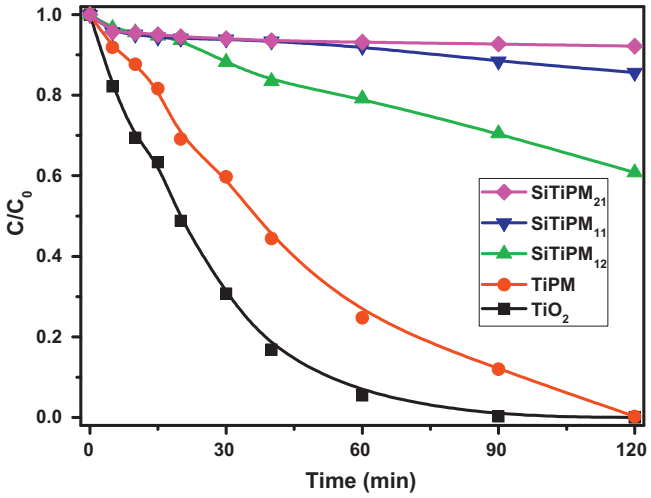

Fig. 5. Photocatalytic degradation kinetics of TCP at the TiO_2 and pillared montmorillonite samples.

3.3. Photocatalytic degradation mechanism of TCP

To better understand the environmental fate and the transformation of TCP at these prepared SiTiPM catalysts, the photocatalytic degradation mechanism of TCP was also investigated. During the degradation, GC/MS is used to identify the main reaction intermediates with or without BSTFA derivatization. The mass spectra and molecular structures of nine degradation intermediates are presented in Fig. S3. Intermediates 1–4 are identified directly from GC/MS as 2,4-dichlorophenol, 2-chloro-1,5-diphenol, 1,3,7-

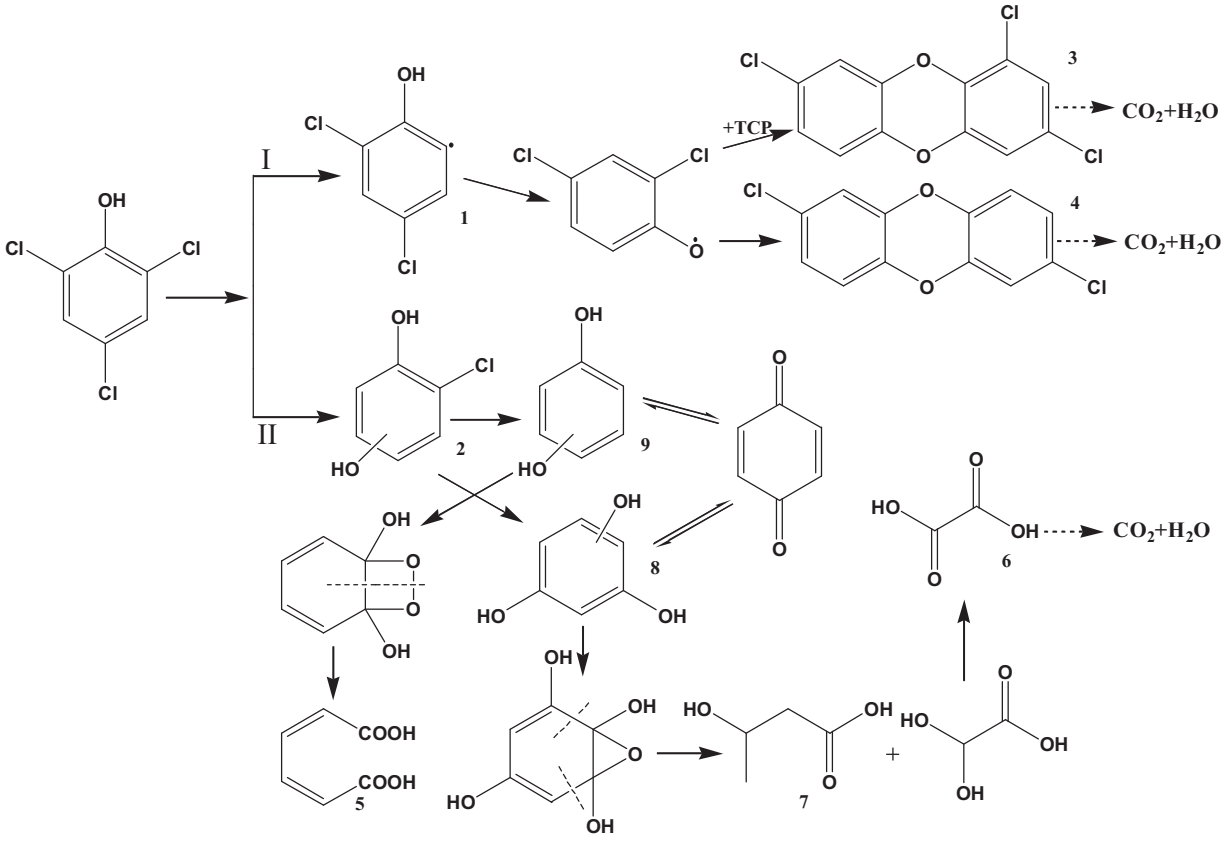

Scheme 1. Proposed reaction mechanism for the photocatalytic TCP degradation.

trichlorodibenzo-p-dioxin, 2,6-dichlorodibenzo-p-dioxin, respectively; while the intermediates 5–9 are detected after silylation derivatization and identified as hexadiene diacid, butyl alkyd, oxalic acid, phloroglucinol and diphenol, respectively. Parts of intermediates are also detected in the previous reports during the photocatalytic degradation of phenols [24–28].

Based on the identified degradation intermediates, a possible photocatalytic degradation mechanism of TCP is proposed in Scheme 1. As shown in the scheme, there are two possible pathways, which may occur simultaneously during photocatalytic process. Following pathway I, the photoinduced electrons generated under the UV illumination initiate nucleophilic attack to the aromatic ring and the cleavage of C–Cl bond happens. Then Cl atom is detached from the benzene ring to generate intermediates 1. Meanwhile, chlorophenols are aggregated to form bicylic compounds such as intermediates 3 and 4. Both of them can be finally completely mineralized into CO_2 and H_2O, etc. in sufficient degradation time. In the pathway II, •OH radicals generated in the solution can also attack the aromatic ring and obtain the OH addition intermediates 2, then follow with the •OH substitution of Cl atom on the ring to obtain intermediates 8 and 9. Likewise, peroxy bond and epoxy bond are also produced, and then further decomposed until the ring is cleaved due to the further attack of •OH radicals to the aromatic ring. Then, a series of ring-opened intermediates such as 5–7 are also detected in the solution. However, with further progress of the degradation reaction, all of the produced intermediates can be eventually mineralized into CO_2 and H_2O.

4. Conclusions

Various SiTiPMs were synthesized by the sol–gel method. The prepared catalysts were used for the adsorption and photocatalytic degradation of hydrophobic organic compound TCP in water. The experimental results indicate that the adsorption capacity of the pillared montmorillonites increased with the increase of the molar ratio of SiO_2 to TiO_2. On the other hand, the larger content of TiO_2 in the pillared montmorillonite resulted in higher photocatalytic activity. The $SiTiPM_{12,}$ with the molar ratio of SiO_2 to TiO_2 of 1:2, possessed the best photocatalytic activity. Two main photocatalytic degradation pathways of TCP including the hydroxylation addition to the parent compound and the Cl atom detached from the benzene ring were proposed.

Acknowledgements

This is contribution No. IS-1264 from GIGCAS. This work was financially supported by the National Natural Science Foundation of China (Nos. 40572173, 40632012 and 40973068).

Appendix A. Supplementary data

Supplementary data associated with this article can be found, the online version, at doi:10.1016/j.cattod.2010.11.014.

References

[1] M.R. Hoffmann, S.T. Martin, W.Y. Choi, D.W. Bahnemann, Chem. Rev. 95 (1995) 69.
[2] A.L. Linsebigler, G.Q. Lu, J.T. Yates, Chem. Rev. 95 (1995) 735.
[3] X. Chen, S.S. Mao, Chem. Rev. 107 (2007) 2891.
[4] Y.Z. Li, S.J. Kim, J. Phys. Chem. B 109 (2005) 12309.
[5] B. Damardji, H. Khalaf, L. Duclaux, B. David, Appl. Clay Sci. 45 (2009) 98.
[6] K.I. Shimizu, T. Kaneko, T. Fujishima, T. Kodama, H. Yoshida, Y. Kitayama, Appl. Catal. A: Gen. 225 (2002) 185.
[7] A. Bhattacharyya, S. Kawi, M.B. Ray, Catal. Today 98 (2004) 431.
[8] J.H. Choy, J.H. Park, J.B. Yoon, J. Phys. Chem. B 102 (1998) 5991.
[9] Z. Ding, H.Y. Zhu, P.F. Greenfield, G.Q. Lu, J. Colloid Interface Sci. 238 (2001) 267.
[10] T.C. An, J.X. Chen, G.Y. Li, X.J. Ding, G.Y. Sheng, J.M. Fu, B.X. Mai, K.E. O'Shea, Catal. Today 139 (2008) 69.
[11] X.F. Meng, Z.Z. Qian, H.T. Wang, X.W. Gao, S.M. Zhang, M.S. Yang, J. Sol–Gel Sci. Technol. 46 (2008) 195.
[12] T.C. An, H. Yang, W.H. Song, G.Y. Li, H.Y. Luo, W.J. Cooper, J. Phys. Chem. A 114 (2010) 2569.
[13] H.Y. Zhu, Z. Ding, C.Q. Lu, G.Q. Lu, Appl. Clay Sci. 20 (2002) 165.
[14] H.M. Zhang, X. Quan, S. Chen, H.M. Zhao, Environ. Sci. Technol. 40 (2006) 6104.
[15] M. Kruk, M. Jaroniec, Chem. Mater. 13 (2001) 3169.
[16] M. Kruk, M. Jaroniec, Y. Yang, A. Sayari, J. Phys. Chem. B 104 (2000) 1581.
[17] T. Endo, M.M. Mortland, T.J. Pinnavaia, Clay Clay Miner. 28 (1980) 105.
[18] S. Yamanaka, Y. Inoue, M. Hattori, F. Okumura, M. Yoshikawa, Bull. Chem. Soc. Jpn. 65 (1992) 2494.
[19] P. Malla, S. Yamanaka, S. Komarneni, Solid State Ionics 32-3 (1989) 354.
[20] S. Yamanaka, P.B. Malla, S. Komarneni, J. Colloid Interface Sci. 134 (1990) 51.
[21] T. Kawai, K. Tsutsumi, Colloid Polym. Sci. 270 (1992) 711.
[22] K. Hayakawa, T. Morita, M. Ariyoshi, T. Maeda, I. Satake, J. Colloid Interface Sci. 177 (1996) 621.
[23] S.W. Lee, H.J. Park, S.H. Lee, M.G. Lee, J. Ind. Eng. Chem. 14 (2008) 10.
[24] U. Stafford, K.A. Gray, P.V. Kamat, J. Phys. Chem. 98 (1994) 6343.
[25] Y.I. Skurlatov, L.S. Ernestova, E.V. Vichutinskaya, D.P. Samsonov, I.V. Semenova, I.Y. Rodko, V.O. Shvidky, R.I. Pervunina, T.K. Kemp, J. Photochem. Photobio. A: Chem. 107 (1997) 207.
[26] C.C. Chen, P.X. Lei, H.W. Ji, W.H. Ma, J.C. Zhao, H. Hidaka, N. Serpone, Environ. Sci. Technol. 38 (2004) 329.
[27] J. Theurich, M. Lindner, D.W. Bahnemann, Langmuir 12 (1996) 6368.
[28] X.J. Li, J.W. Cubbage, T.A. Tetzlaff, W.S. Jenks, J. Org. Chem. 64 (1999) 8509.

Supporting Information

Synthesis and Characterization of Novel SiO_2 and TiO_2 Co-pillared Montmorillonite Composite for Adsorption and Photocatalytic Degradation of Hydrophobic Organic Pollutants in Water

Jiangyao Chen[a,c], Xiaolu Liu[a,c], Guiying Li[a], Xin Nie[a,c], Taicheng An[a,*], Shanqing Zhang[b], Hunjun Zhao[b]

[a] *State Key Laboratory of Organic Geochemistry, Guangdong Key Laboratory of Environmental Resources Utilization and Protection, Guangzhou Institute of Geochemistry, Chinese Academy of Sciences, Guangzhou 510640, China;*

[b] *Environmental Futures Centre and Griffith School of Environment, Gold Coast Campus, Griffith University, QLD 4222, Australia;*

[c] *Graduate School of Chinese Academy of Sciences, Beijing 100049, China.*

*Corresponding author, Prof. Taicheng An, Tel: +86-20-85291501; Fax: +86-20-85290706; E-mail: antc99@gig.ac.cn

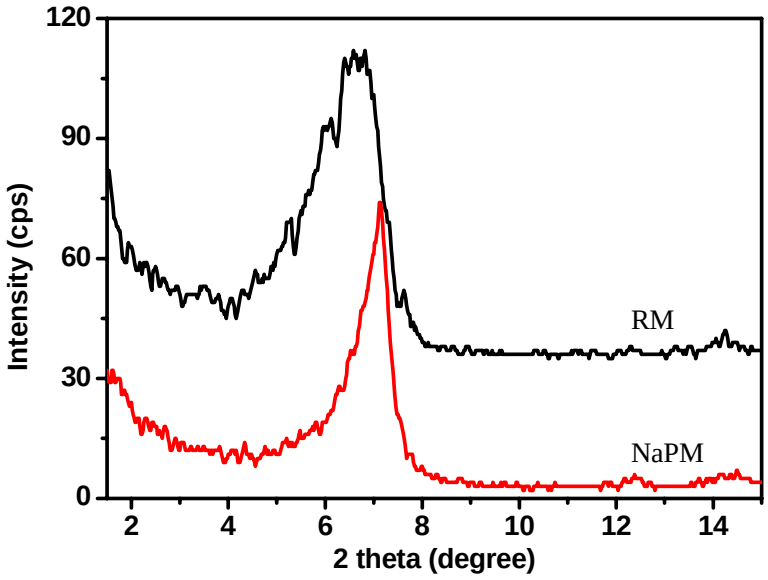

Fig. S1. Small angle XRD patterns of the RM and NaPM samples

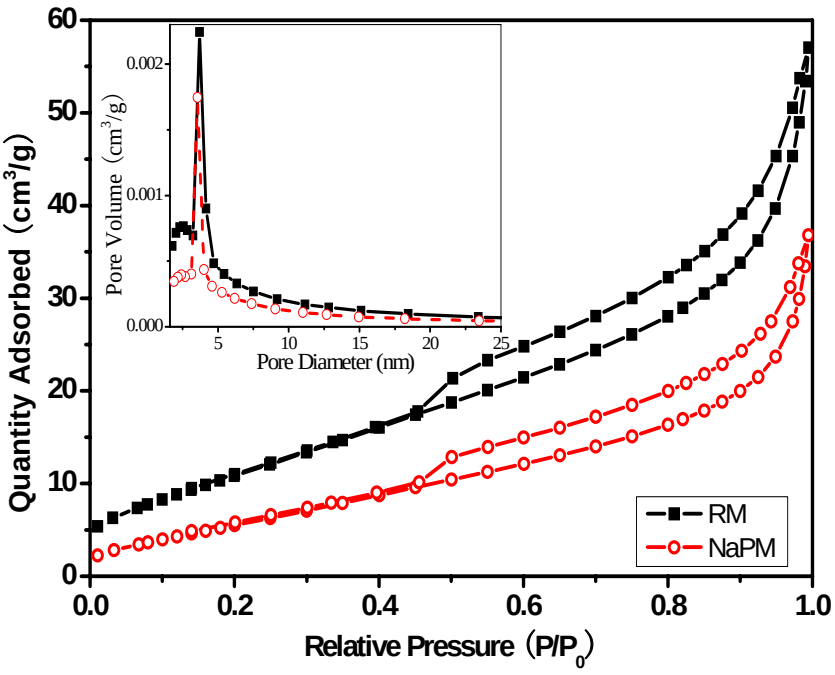

Fig. S2. The N_2 adsorption/desorption isotherms and BJH desorption pore size distributions of the RM and NaPM

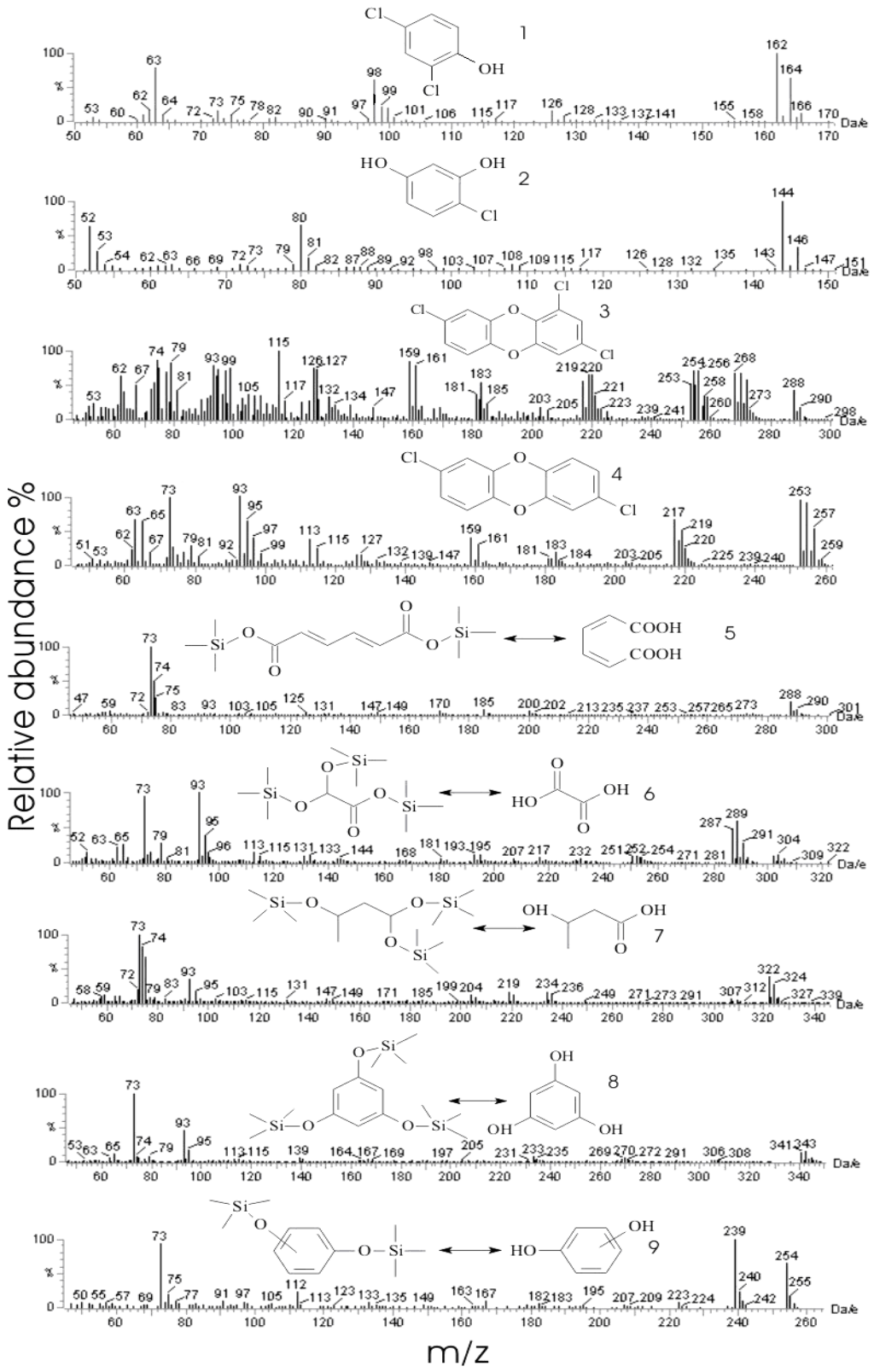

Fig. S3. Mass spectra of the intermediates found in the photocatalytic TCP degradation process.